Large-eddy simulation of flow over a circular cylinder in the sub-critical regime

W. Cheng

Mechanical Engineering,
Physical Sciences and Engineering Division
King Abdullah University of Science and Technology
Thuwal, Saudi Arabia
wan.cheng@kaust.edu.sa

D. I. Pullin

Graduate Aerospace Laboratories
California Institute of Technology
1200 E. California Blvd.
Pasadena CA 91125
dpullin@caltech.edu

R. Samtaney

Mechanical Engineering, Physical Sciences and Engineering Division
King Abdullah University of Science and Technology
Thuwal, Saudi Arabia
ravi.samtaney@kaust.edu.sa

ABSTRACT

We present wall-resolved, large-eddy simulation (LES) of flow over a circular cylinder up to $Re_D = 10^5$, based on the cylinder diameter D, in the subcritical regime. The numerical method is a fully centered-finite-difference scheme on a standard curvilinear O-grid. The stretched-vortex sub-grid scale model is used in the whole domain, including regions of large-scale separated flow. Both second- and fourth-order accurate schemes are used separately, and results, specifically the skin-friction coefficient along the cylinder surface and its variation with Re_D, are compared with literature data.

1 Introduction

The flow of a Newtonian fluid over a cylinder is known to exhibit an interesting range of physical phenomena. With increasing $Re_D \equiv U_\infty D/\nu$ where U_∞ the free-stream velocity and ν the kinematic viscosity, the flow develops from steady and stable with a closed wake, to two-dimensional unsteady flow and then to three-dimensional flow following wake transition, shear-layer transition and possible boundary-layer transition. Beyond some critical Reynolds number Re_C (around $Re_D = 10^3$), the flow is observed to become turbulent owing to Kelvin-Helmholtz instability of the two shear layers that separate from the cylinder surface. The flow with $Re_D = 3900$ exceeds Re_C and is perhaps the most documented benchmark case in the literature. Some experimental studies at this Re_D focus on the character of the near-wall flow including Norberg (1993), who documents pressure-coefficient measurements, while others, for example Lourenco & Shih (1994), report results for mean velocity and turbulent intensity profiles in the near-wake region.

Above Re_C, the flow is typically characterized as having entered the subcritical regime where turbulence in the wake flow gets stronger and moves upstream with increasing Re_D. In this regime, some general tendencies can be observed for increasing Re_D, including increasing drag coefficient C_D and shrinking of the recirculation length. Weidman (1968) studied the flow in this the subcritical Re_D range, finding that the pressure minima are only weakly dependent on Re_D in the range $Re_D = 10^4$ to 10^5. There are however, limited numerical simulation results available in this regime that address in detail the near-wall flow, especially the variation of the skin-friction C_f around the cylinder surface. This is expected to be important for understanding high Reynolds-number, bluff-body flows, where the near-wall velocity gradient at some fixed station generally increases with Re_D.

In the present work, we study the behavior of the wall skin friction at different Re_D. Related flow-separation behavior is also discussed. Of particular interest is the performance of similar numerical schemes with different order of accuracy.

2 Numerical method

The LES equations with an explicit sub-grid scale model were solved using a semi-implicit fractional step method. Spatial discretization of the nonlinear term utilizes either a second- or fourth-order energy-conservative skew-symmetric form (Morinishi *et al.*, 1998) while for all other terms, consistent second/fourth-order central differences were used. The modified Helmholtz equations that arise from implicit treatment of viscous terms, a pressure Poisson equation and the velocity-correction step are solved successively. The code has been tested using DNS of airfoil flow (Zhang *et al.*, 2015) and also a also flow over a square cylinder with rounded corners (Zhang & Samtaney, 2016).

The subgrid-scale model is the stretched-vortex (SV) model (Misra & Pullin, 1997; Voelkl *et al.*, 2000; Chung & Pullin, 2009), where the subgrid flow is modeled by tube-like structures that are stretched by the eddies comprising the local resolved-scale flow. The LES are wall-resolved where the wall-normal resolution nowhere exceed $1-2$ times the wall-viscous length scale ν/u_τ where u_τ the local friction velocity.

3 Cases and results

All LES discussed presently employ the same domain: $L_z = 3D$ and $L_r = 40$. Cases and corresponding meshes are listed in Table 1.

Case 0: $Re_D = 3900$

First we discuss the benchmark case with $Re_D = 3900$. In order to appreciate how the two numerical schemes perform in a relative sense, it is useful to study the flow development starting from time $t = 0$. In figure 1, we show the time-wise evolution of both the drag coefficient C_D and lift or side-force coefficient C_L for two simulations. It can be seen that, with a given initial condition, the flow for

Case	Re_D	N_θ	N_r	N_y	*Scheme*
$C0S$	3900	256	256	64	2^{ed}
$C0F$	3900	256	256	64	4^{th}
$C1S$	10^4	384	384	96	2^{ed}
$C1F$	10^4	384	384	96	4^{th}
$C2S$	10^5	1024	512	256	2^{ed}
$C2F$	10^5	1024	512	256	4^{th}

Table 1. LES performed. N_i is the mesh number in the 'i' direction.

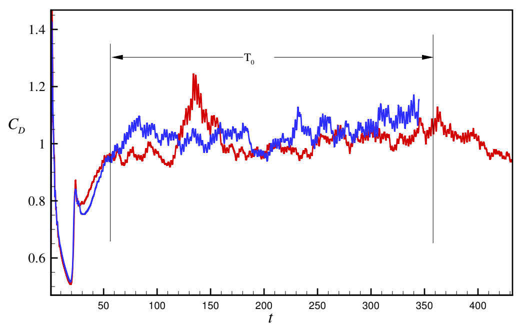

(a) drag coefficient

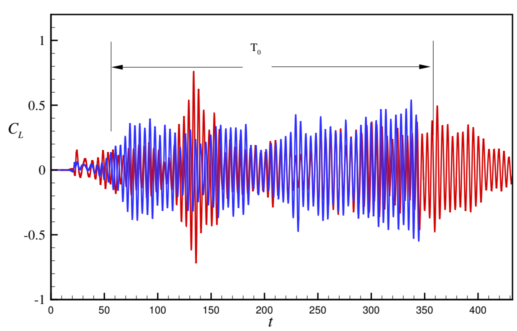

(b) lift coefficient

Figure 1. $Re_D = 3900$: time evolution of drag coefficient C_D and lift coefficient C_L. ——— (blue), case $C0S$; ——— (red), case $C0F$.

both LES first experiences a transient period, up to about $t = 50$, followed by the development of a shedding state. Differences between two schemes for $t > 30$ are clear. In the diagnostic period, marked as T_0 , $C_D(t)$ shows somewhat different instantaneous evolution for the two cases but numerically similar time-averages, while $C_L(t)$ exhibits quite similar local behavior in every shedding period, except in one window, $120 < t < 150$. For quantitative comparison, we list the time-averaged drag coefficient C_D, Strouhal number *St* and the recirculation length L_B in table 3. Both results match the literature data reasonably well. The difference between results from two schemes are sufficiently small so as to be considered as the effects of truncation error.

We compare results of the present LES with the experimental data of Parnaudeau *et al.* (2008), the LES results of Kravchenko & Moin (2000) and DNS results (case II) of Ma *et al.* (2000). In figure 2, we plot the mean stream-wise velocity along the y direction at $x = 1.06$. We can conclude that the differences between

Case	C_D	*St*	L_B
$C0S$	1.06	0.213	1.32
$C0F$	1.04	0.211	1.31
Exp.	0.98 ± 0.05	0.215 ± 0.005	1.33 ± 0.02

Table 2. Comparison of LES results with experimental data at $Re_D = 3900$. For experiment data, C_D from Norberg (1993), *St* and L_B from Cardell (1993) .

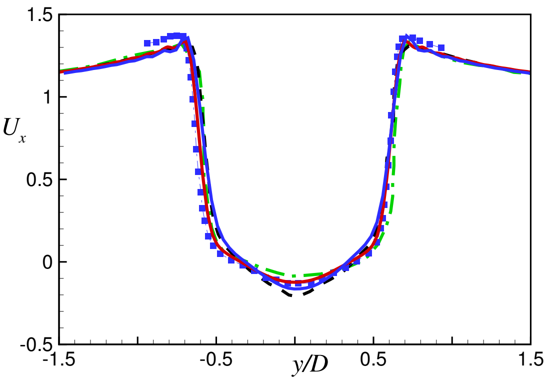

Figure 2. $Re_D = 3900$: comparison of mean streamline velocity U_x. ——— (red), present LES $C0F$; ——— (blue), present LES $C0S$; ■ , experiments by Parnaudeau *et al.* (2008); —·— , LES by Beaudan & Moin (1994) - - - - , DNS by Ma *et al.* (2000).

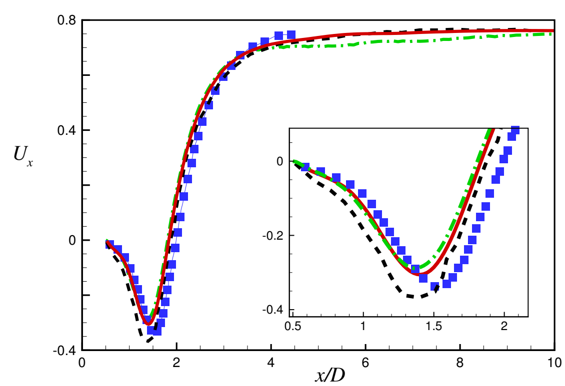

Figure 3. $Re_D = 3900$: comparison of U_x along the centerline. ——— (red), present LES $C0F$; —·— (blue), present LES $C0S$; ■ , experiments by Parnaudeau *et al.* (2008); - - - - , LES by Beaudan & Moin (1994).

different simulation results and experiment are small and at approximately the same level. The present LES $C0F$ agrees quite well with Kravchenko & Moin (2000) except at around $y/D = 0$. Near the centerline $y/D = 0$, it matches the valley value of U_x from experiments. For case $C0S$, the velocity profile shape somewhat tends to the result of Ma *et al.* (2000), but the U_x valley value is still close to the experiment and LES by Kravchenko & Moin (2000). We also compare the stream-wise mean velocity in the wake centerline, as shown in figure 3. All simulation results generally capture the behavior of the U_x distribution, which first decreases to a minimum value, then recovers monotonically in the far wake region. We note

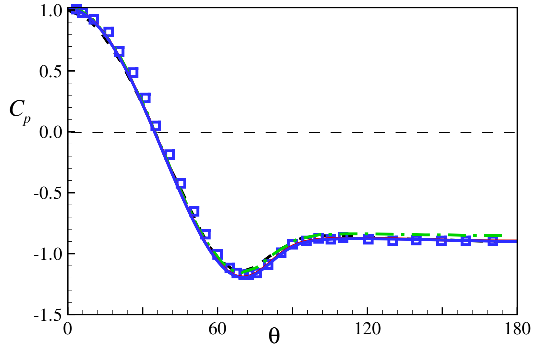

(a) pressure coefficient

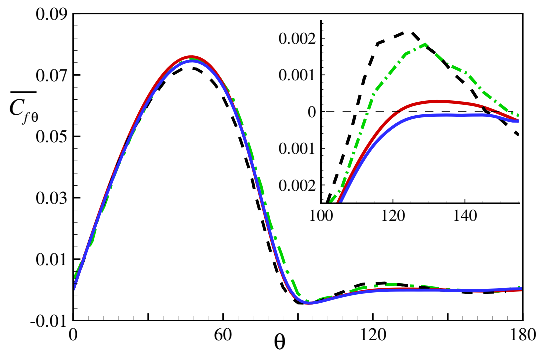

(b) skin friction coefficient

Figure 4. $Re_D = 3900$: comparison of pressure coefficient and skin friction coefficient. ——— (red), present LES $C0F$; ——— (blue), present LES $C0S$; □, experiments by Norberg (1993); —·—, LES by Beaudan & Moin (1994) - - - -, DNS by Ma *et al.* (2000).

that in the region of decrease, the present LES, both $C0S$ and $C0F$, agree well with the experimental data, while in the recovery region up to $x/D \approx 4$, the present LES and the LES result by Kravchenko & Moin (2000) are in reasonable agreement both with each other and with experiment by Parnaudeau *et al.* (2008). Further downstream, $C0F$ is found to closely follow the LES result by Kravchenko & Moin (2000) while $C0S$ shows an obvious deficit. This deviation weakens with x/D and is finally close to the result of case $C0F$. This can probably be ascribed to use of an overly coarse mesh. For the high-order numerical scheme, the present mesh is sufficient to give accurate results while for the second-order scheme, sub-grid terms are perhaps insufficient to model the real physics.

The pressure coefficient C_p is shown in figure 4(a) where it can be seen that all results agree reasonably well. The relative difference between the present LES and the experimental data is roughly 3% at about 70°; the difference between two cases $C0S$ and $C0F$ is so small that the two lines almost overlap. Additionally we compare $C_{f\theta}$ along the cylinder surface with experiment and previous simulations in figure 4(b). All $C_{f\theta}$ distributions show good agreement. In the closeup inset of 4(b), we can see that three of the simulations show a mean-flow secondary-separation bubble whose size and location differs for the cases shown. The exception is the $C0S$ LES that does not clearly capture a mean-flow separation bubble. The LES of $C0F$ shows reattachment of the secondary-separation bubble at about $\theta > 120°$ from the windward stagnation line, which is larger than values given by the other two cases. In contrast, for the mean-flow separation position of the secondary-separation bubble, all simulations give similar results at around $\theta = 150°$. Son & Hanratty (1969) found that the reattachment angle for the secondary

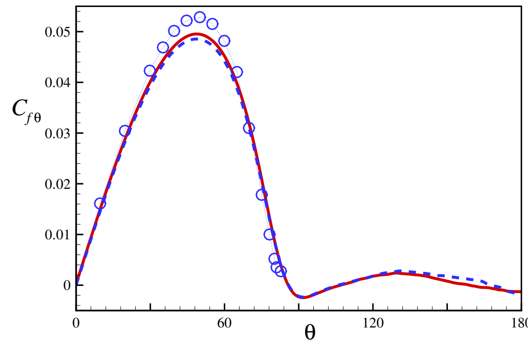

(a) $Re_D = 10^4$

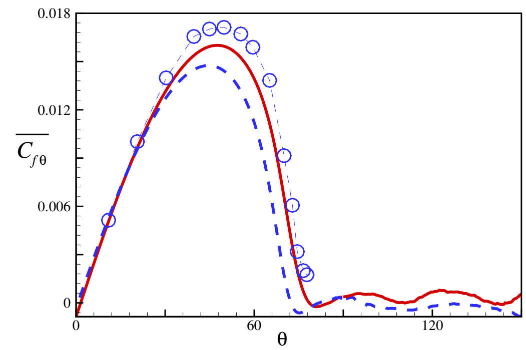

(b) $Re_D = 10^5$

Figure 5. Comparison of skin friction coefficient. ——— (red), present LES $C0F$; - - - - (blue), present LES $C0S$; ○, Son & Hanratty (1969).

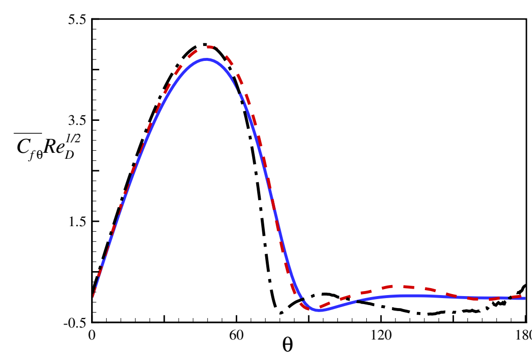

Figure 6. Scaled skin friction coefficient. Re_D : ———, 3900; - - - -, 10^4; —·—, 10^5.

bubble decreases with increasing Reynolds number. At $Re_D = 5000$ it is about 120°. Extrapolating their results suggests a separation angle slightly larger than 120° at $Re_D = 3900$. This agrees with the present LES calculations and is rather larger than 110° seen in other simulation results.

Subcritical regime: case 1 and case 2

LES for $Re_D = 10^4$ and 10^5, as listed in Table 1 were performed. In figure 5 we compare $C_{f\theta}$ with experimental data by Son & Hanratty (1969). For $Re_D = 10^4$, 10^5, the second-order method reproduces the wall stress reasonable well, but for $Re_D = 10^5$, this scheme does not accurately capture the separation behavior. This indicates that, for the second-order scheme at higher Re_D, a finer

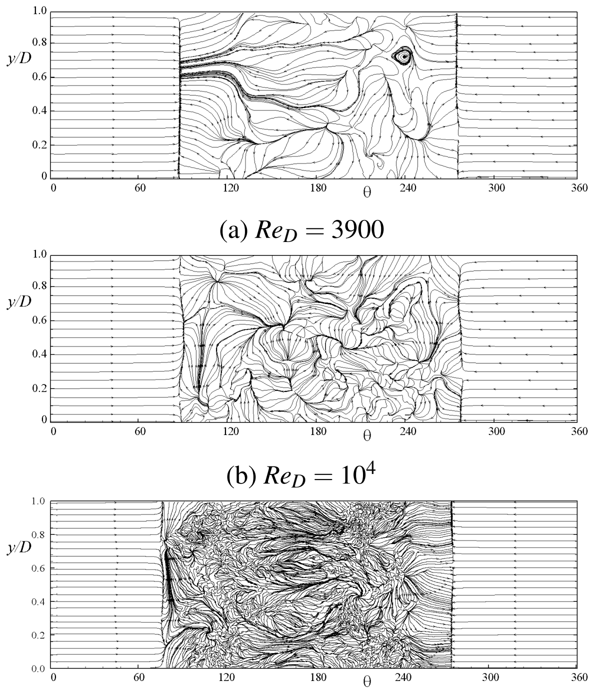

(a) $Re_D = 3900$

(b) $Re_D = 10^4$

(c) $Re_D = 10^5$

Figure 7. Skin friction lines of instantaneous C_f.

mesh is required than used presently for results to be consistent with those of the fourth-order scheme.

According to Son & Hanratty (1969) $C_{f\theta}Re_D^{1/2}$ should provide proper scaling for the re-attached flow. In figure 6, this is shown for all three cases using the fourth-order scheme. Another interesting phenomenon observed from figure 6 is the decrease of the separation angle with increasing Re_D. For the LES with $Re_D = 10^5$, the separation angle is about 75°, which shows reasonable agreement with existing experimental data, for example, Achenbach (1968), who measured 78° at $Re_D = 10^5$.

It is also of interest to examine the instantaneous surface trajectory field for $\mathbf{C_f}$. In these images, the circular cylinder surface is cut along the front stagnation line $\theta = 0$ and then unfolded onto a flat surface. The flow is therefore onto the cylinder surface at both $\theta = 0$ and $\theta = 360°$. In figure 7(a), the surface $\mathbf{C_f}$ field for $Re_D = 3900$ shows almost straight skin-friction lines prior to flow separation corresponding to the attached boundary layer flow on the front part of the cylinder. Separation can be observed at about $\theta = 90°$ and $\theta = 270°$, where skin friction lines reveal several critical points defined as surface points where $\mathbf{C}_f = 0$. In the large-scale separated-flow region, further critical points can be observed. Surface $\mathbf{C_f}$ surface trajectories are shown for $Re_D = 10^4$ in figure 7(b). Here the primary separation lines show somewhat two-dimensional behavior. Inside the separation region, the area density of critical points is larger than for $Re_D = 3900$. The surface $\mathbf{C_f}$ field of 7(c) at $Re_D = 10^5$ shows a rather different pattern in the separated-flow region. Around the rear stagnation point (about $150° < \theta < 210°$), clear bifurcation lines, where the neighboring skin friction lines asymptote, can be seen. The area density of critical points in the separated-flow region is now increased in comparison with the $Re_D = 10^4$ LES. Interestingly, in both cases, it is difficult to identify instantaneous flow features that clearly correspond to the mean-flow secondary-separation bubble. This is reminiscent of separation and reattachment in a flat plate turbulent boundary layer flow as shown by Chong *et al.* (1998), where the separation/reattachment points are ambiguous in the plot of the surface $\mathbf{C_f}$ field.

4 Conclusion

We have reported results from wall-resolved large-eddy simulation for flow past a circular cylinder in the sub-critical regime with $Re_D = 3900$, 10^4 and 10^5. These LES were performed with both second-order and is fourth-order finite difference schemes. For $Re_D = 3900$, mean velocity profiles and some near-wall properties are discussed. At this Re_D, both schemes give satisfactory results. For the LES at $Re_D = 10^5$, the present mesh is sufficiently fine for the accurate capturing of salient flow features using the fourth-order scheme. A finer mesh would be necessary for the present second-order scheme to produce results comparable to those of the four-order method..

REFERENCES

Achenbach, E. 1968 Distribuion of local pressure and skin friction around a circular cylinder in cross-flow up to Re=5×10^6. *Journal of Fluid Mechanics* **34**, 625–639.

Beaudan, P. & Moin, P. 1994 Numerical experiments on the flow past a circular cylinder at sub-critical Reynolds number. *Tech. Rep.* TF-62. Stanford Univerisity.

Cardell, G. S. 1993 Flow past a circular cylinder with a permeable splitter plate. PhD thesis, California Institute of Technology.

Chong, M. S., Soria, J., Perry, A. E., Chacin, J., Cantwell, B. J. & Na, Y. 1998 Turbulence structures of wall-bounded shear flow found using dns data. *J. Fluid Mech.* **357**, 225–247.

Chung, D. & Pullin, D. I. 2009 Large-eddy simulation and wall modelling of turbulent channel flow. *J. Fluid Mech.* **631**, 281–309.

Kravchenko, A. G. & Moin, P. 2000 Numerical studies of flow over a circular cylinder at $re_d = 3900$. *Physics of Fluids* **12**, 403–417.

Lourenco, L. M. & Shih, C. 1994 Characteristics of the plane turbulent near wake of a circular cylinder, a particle image velocimetry study. *Tech. Rep.* TF-62. Stanford Univerisity, by Beaudan P. and Moin P.

Ma, X., Karamanos, G. S. & Karniadakis, G. E. 2000 Dynamics and low-dimensionality of a turbulent near wake. *Journal of Fluid Mechanics* **410**, 29–65.

Misra, A. & Pullin, D. I. 1997 A vortex-based subgrid stress model for large-eddy simulation. *Phys. Fluids* **9**, 2443–2454.

Morinishi, Y., Lund, T. S., Vasilyev, O. V. & Moin, P. 1998 Fully conservative higher order finite difference schemes for incompressible flow. *Journal of Computational Physics* **143**, 90–124.

Norberg, N. 1993 Pressure forces on a circular cylinder in cross flow. In *IUTAM Symposium Bluff-Boday Wakes, Dynamics and Instabilities*.

Parnaudeau, P., Carlier, J., Heitz, D. & Lamballais, H. 2008 Experimental and numerical studies of the flow over a circular cylinder at Reynolds number 3900. *Phys. Fluids* **20**, 085101.

Son, J. S. & Hanratty, T. J. 1969 Velocity gradients at the wall for flow around a cylinder at Reynolds numbers from 5×10^3 to 10^5. *Journal of Fluid Mechanics* **35**, 353–368.

Voelkl, T., Pullin, D. I. & Chan, D. C. 2000 A physical-space version of the stretched-vortex subgrid-stress model for large-eddy simulation. *Phys. Fluids* **228**, 2426–2442.

Weidman, P. 1968 Wave transition and blockage effects on cylinder base pressures. PhD thesis, California Institute of Technology.

Zhang, W., Cheng, W., Gao, W., Qamar, A. & Samtaney, R. 2015 Geometrical effects on the airfoil flow separation and transition. *Comput. Fluids* **15**, 60–73.

Zhang, W. & Samtaney, R. 2016 Low-Re past an isolated cylinder with rounded corners. *Comput. Fluids* **136**, 384–401.